processes

MDPI

Article

Chemical Interaction of Cr-Al-Cu Metal Powders in Aluminum-Assisted Transfer of Chromium in Submerged Arc Welding of Carbon Steel

Theresa Coetsee * and Frederik De Bruin

Department of Materials Science and Metallurgical Engineering, University of Pretoria, Pretoria 0002, South Africa; fjdb.1953@gmail.com
* Correspondence: theresa.coetsee@up.ac.za

Abstract: In submerged arc welding (SAW) of chromium containing steels, the chromium in the weld metal is usually sourced from weld wire. Manufacturing of precise weld wire compositions for alloying of the weld metal is expensive. In addition, alloying of weld metal with high levels of copper via weld wire is hindered by work hardening of the weld wire. In the SAW process, a large quantity of oxygen is added to the weld pool. Because chromium has a high affinity for oxygen, the oxygen partial pressure at the weld pool-molten flux interface must be controlled to ensure high recovery of chromium to the weld metal. This study illustrates the application of copper as stabilizer, in conjunction with aluminum, to enhance chromium transfer to the weld pool. The stabilizer effect occurs because the Cr-Al-Cu alloy liquidus temperatures are much lower than the pure Cr liquidus temperature. The result is an increase in the total quantity of Cr, Al, and Cu powder melted into the weld pool. The application of Al powder additions to control the partial oxygen pressure at the molten flux-weld pool interface is confirmed in the presence of Cr and Cu metal powders to ensure the weld metal ppm O content is maintained at the acceptable level of 300 ppm.

Keywords: oxygen potential; chromium; aluminum; copper; metal powder; submerged arc welding

check for updates

Citation: Coetsee, T.; De Bruin, F. Chemical Interaction of Cr-Al-Cu Metal Powders in Aluminum-Assisted Transfer of Chromium in Submerged Arc Welding of Carbon Steel. *Processes* **2022**, *10*, 296. https://doi.org/10.3390/pr10020296

Academic Editor: Prashant K Sarswat

Received: 8 January 2022
Accepted: 30 January 2022
Published: 1 February 2022

Publisher's Note: MDPI stays neutral with regard to jurisdictional claims in published maps and institutional affiliations.

Copyright: © 2022 by the authors. Licensee MDPI, Basel, Switzerland. This article is an open access article distributed under the terms and conditions of the Creative Commons Attribution (CC BY) license (https://creativecommons.org/licenses/by/4.0/).

1. Introduction

Submerged arc welding (SAW) is applied in heavy engineering industries to weld thick steel plate sections [1]. Electrical current is passed between the continuously fed weld wire tip and the steel base plate to generate an arc which drives the complex chemical and electrical processes in SAW. Welding flux is continuously fed with the weld wire. The layer of flux nearest to the arc plasma volume is melted to slag which shields the arc cavity from air ingress and limits arc energy losses to the environment. As the weld wire is fed into the arc cavity, it melts into droplets which are transferred to the weld pool. The SAW process in the arc cavity and in the trailing weld pool consists of complex interactions of physical and chemical phenomena of heat and mass transfer [1,2]. The overall SAW chemical reaction time is set by the steel solidus temperature because chemical reactions between the molten weld pool and its covering slag may continue as long as the weld metal remains partially molten [3,4]. The welding flux usually contains a blend of oxides and fluoride minerals of which CaF_2 is most often used. It has been empirically determined that the weld metal total oxygen content, and hydrogen content, are maintained at low levels if the flux composition is specified to ensure that the basicity index (BI) is held higher than 1.5, see Equation (1) for Tuliani's BI index expression [5,6]. Flux component percentages in Equation (1) are in mass%.

$$BI = \frac{[\%CaF_2 + \%CaO + \%MgO + \%BaO + \%SrO + \%Na_2O + \%K_2O + \%Li_2O + 0.5(\%MnO + \%FeO)]}{[\%SiO_2 + 0.5(\%Al_2O_3 + \%TiO_2 + \%ZrO_2)]} \quad (1)$$

Previous studies demonstrated that the droplets of molten weld wire transfer large quantities of oxygen (2000–3000 ppm O) into the weld pool via the weld pool-arc plasma interface [7,8]. The molten weld wire droplets retained oxygen from the decomposition of less stable oxides in the arc plasma. Less stable oxides decompose more readily in the arc plasma due to high temperatures prevailing in the arc plasma. Therefore, flux chemistry specification is an important control input in the SAW process to set the quantity of transferrable oxygen released in the arc plasma [9]. Binary CaF_2-oxide flux mixtures were used in SAW tests to determine the arc stability hierarchy of the individual oxides. It was found that the oxide stability hierarchy increased from MnO and SiO_2, to MgO, Al_2O_3, TiO_2, and Na_2O, K_2O, and CaO as the most stable oxide in the arc plasma [9]. Since the weld metal oxygen is sourced from oxides contained in the flux, a generally accepted method of lowering the weld metal ppm oxygen is to increase the flux CaF_2 content in order to dilute the quantity of oxides in the flux. Weld metal impact toughness in carbon steels is dependent on the weld metal oxygen content, and therefore the weld metal oxygen must be controlled within a narrow band. The literature reported guideline on acceptable weld metal oxygen content levels for sufficient weld metal impact toughness is oxygen content levels higher than 200 ppm O and lower than 500 ppm O [10]. Several previous studies concluded that large quantities of oxygen from flux oxide dissociation in the arc plasma is transferred via molten weld wire droplets to the arc plasma-weld pool interface, where this oxygen and iron react to form FeO in the colder weld pool steel. The formed FeO is absorbed into the molten flux (slag) at the weld pool-molten flux interface. The established correlation is that the weld metal ppm O increased with increased FeO in the molten flux [11–16].

Notably, the arc plasma stability of Cr-oxides, CrO, and Cr_2O_3 were not tested in the above-mentioned work [9]. Therefore, the arc stability of the Cr-oxides is not clear. One of the main chemical design considerations in flux design is to ensure that specific weld metal alloying elements are transferred from the molten flux to the weld pool. For example, the Si and Mn content level in low alloy carbon steels may be increased by increasing the flux SiO_2 and MnO content, respectively. Description of the flux alloying behavior is then described as high, moderate, or low alloying with respect to Si or Mn [17].

Chromium is added to low alloy steels to improve the oxidation resistance of steel and improve the steel tensile strength at elevated service temperatures beyond 345 °C. For example, chromium-molybdenum steels containing 9% Cr and 1% Mo are used to construct pressure vessels and pipelines for high temperature applications, such as thermal power plant applications [18,19]. Stainless steels contain in excess of 11% Cr to improve steel corrosion resistance. Most stainless-steel grades may be welded by SAW [19]. Chromium is typically added to the weld metal from the weld wire, and the weld wire chemistry is usually over matched to the base plate composition. Consequently, the fluxes are neutral or non-alloyed [17]. Minor quantities of chromium, nickel, molybdenum, or niobium may be added as metallic powders in the flux formulation to compensate for arc losses of these elements [19]. Manufacturing of weld wires of specific compositions is expensive and time consuming and cannot closely match all desired alloy compositions. Therefore, the use of chromium weld wire to add large quantities of chromium to the weld metal to match the base plate composition is not easily accomplished. This objective may be better accomplished if the weld metal incorporates metal powder to attain the desired composition. Copper is increasingly added to carbon steels and stainless steels to enhance mechanical and corrosion properties [20]. For example, copper is added to chrome-manganese stainless steels to relatively high levels of 4% for improved steel corrosion resistance, whilst maintaining good weldability [20]. However, copper addition to weld wire causes work hardening of the weld wire. The materials handling consequence is that the copper containing alloy is

not easily formed into wire product, and it is also not easily passed through the roller guide system of the SAW equipment [21]. Addition of copper to the weld metal in SAW as metal powder offers a solution to the practical materials problem of feeding work hardening copper containing wire.

Recently the concept of low density/high-entropy steels have emerged to improve the steel material properties through high alloy additions to Fe to improve steel tensile strength and ductility at the same time, as in the case for high-entropy alloys (HEAs) [22]. Aluminum is used to lower steel density and also to induce the high entropy-effect in these steel formulations initially focused on the Fe-C-Mn-Al-Si chemical system [23]. Similarly, lightweight stainless steels are formulated by adding about 10% Al to Fe-Mn-Cr formulations [24]. The problem of matching weld consumables to the base plate material is also found in steel of lower alloying additions. For example, in GMA (gas metal arc) welding of high-strength fine grain structural steels the addition of high oxygen affinity metals such as Al, Zr, Cr, and Ti to the desired levels is challenging as varied weld wire chemistries are required. Consequently, new technologies are developed to add these elements cost effectively to solid weld wire, such as magnetron sputtered coatings [25].

Therefore, a method of welding low density/high-entropy steels with weld metal of the same composition is an important developmental target in utilizing high-entropy steels in manufacturing. Since SAW is used to achieve high production productivity, the expansion of the application of SAW to a wide class of newly developed alloys and steels will be a benefit to the engineering industry. The method of alloying the weld metal to the desired composition must be matched to the specific alloying element's chemical behavior and the interaction between the selected alloying elements. Alloying of the weld metal with Al and Ti is hampered due to difficulty in transferring these elements across the welding arc [19]. Therefore, addition of Al via weld wire is unlikely workable due to the high affinity of Al for oxygen. Considering some of the alloying examples above, it is likely that copper and chromium, in combination with Al, will be added to new steel and alloy grades to improve materials properties; and in welding of these material grades to match the weld metal to the steel chemistry and materials properties.

There are some reported studies on the use of unconstrained (not fluxed cored or metal cored wire) metal powders in SAW. These applications are geared towards the use of high Fe content powders to increase welding productivity in welding joint applications, and in cladding applications [26–28]. To the authors' knowledge there are only a limited number of published studies in which mention is made of the application of unconstrained metal powders in SAW to generate a highly alloyed weld metal [27–29]. Knowledge on the behavior of the different alloying elements in the SAW process in terms of interaction with oxygen and added powder alloy elements is required to be able to successfully apply unconstrained metal powders to alloy the weld metal. Thus, the purpose of this work is to illustrate the application of copper metal powder addition in SAW to stabilize the Al and Cr powder metal uptake into the weld metal, and still control the ppm O in the weld metal within the target of 200–500 ppm O.

2. Materials and Methods

2.1. Welding Experiments

Three experimental scenarios were used to compare the process effects of addition of Al and Cr metal powder to the weld metal (MP2), to addition of Al, Cr, and Cu metal powder to the weld metal (MP4), and to the base case (BC) experiment with no metal powder addition. The results from these experiments confirm the method of oxygen potential control at the molten flux-weld pool interface via Al metal powder, in the presence of Cr and Cu metal powders in unconstrained format.

Bead-on-plate welds were made onto structural steel plates (EN 10025-2). Each weld test was made on a separate base plate, along the length of the plate. The base plate dimensions were 350-mm-length by 12-mm-thickness by 300-mm-width. The welding equipment used is the most commonly used SAW equipment set-up type for welding

with a single solid wire, namely a DC (direct current) constant-voltage power source [19]. The welding equipment consists of a Lincoln Electric IDEALARC® DC-600 power source linked to a Lincoln Electric NA-3N solid state automatic wire feeder. Weld parameters were 500 A, 28 V, and 42 cm/minute travel speed for 2.0 kJ/mm weld heat input at DCEP (Direct Current Electrode Positive) and using 3.2 mm diameter weld wire. The mixed unconstrained metal powders of 10 g each were used per weld run [30].

2.2. Input Materials

Table 1 shows the base plate major element analysis as made by optical emission spectroscopy (OES), and the weld wire analysis from the supplier's specification sheet (Afrox Ltd., Johannesburg, South Africa). Both base plate and weld wire oxygen and carbon content were analyzed by combustion method.

Table 1. Steel base plate and weld wire compositions.

	%C	%Si	%Mn	%Cr	%Fe	%Cu	* O	%Al	%P	%S	%Ti
Plate	0.120	0.155	1.340	0.160	98.21	0.030	71	0.067	0.019	0.007	0.005
Wire	0.110	0.137	0.990	0	98.75	0.140	30	0	0.009	0.023	0

* ppm; % is in mass%; balance is Fe.

A commercial agglomerated flux was selected for this work following prior detailed investigation on different commercial fluxes' mineralogy, chemistry, and slag phase chemistry [11,31]. The main consideration was flux stability in the presence of Al powder added as de-oxidizer into the weld pool. The bulk composition of the selected aluminate basic flux (basicity index (BI) = 1.4) is shown in Table 2 [11,31].

Table 2. Flux composition (mass%).

MnO	CaO	SiO_2	Al_2O_3	CaF_2	MgO	FeO	TiO_2	Na_2O	K_2O
7.1	0.1	20.4	25.9	18.0	23.1	2.5	1.0	1.7	0.2

The metal powder additions were sourced as Al (99.7% Al) supplied by Sigma Aldrich (St. Louis, MO, USA), Cr (99.0% Cr) as supplied by Alfa Aesar and Cu (99.8% Cu) supplied by Goodfellow.

2.3. Weld Metal Analyses

Weld metal cross sections were made at three different positions at the center position of the weld run. Three cross sections were used for major element analysis by optical emission spectroscopy (OES). Volume samples were cut from the cross sections for oxygen and carbon analyses by combustion method.

One weld metal cross section was prepared as a polished section to check the bulk composition with area analysis of the alloy by SEM (scanning electron microscope), using EDS (energy dispersive spectrometer) analysis. Following polishing, the sample was etched with 2% Nital solution to show the weld metal and heat affected zone. The SEM equipment used is a Zeiss crossbeam 540 FEG (Field emission gun) with EDS (energy dispersive spectrometer) analysis done at 20-kV and 5.6-mm working distance.

2.4. Slag Analyses

Post-weld slags were collected from the whole weld run length. The bulk slag chemistry was analyzed by Inductively Coupled Plasma Optical Emission Spectroscopy (ICP-OES) for all elements except for F, which was analyzed by titration method.

3. Results

The average weld metal composition from three samples per weld run are summarized in Table 3. Three welding test scenarios are reported: the base case (BC) in which no metal powders were added to the weld metal, MP2 weld metal formed with Al and Cr metal powder addition, and MP4 weld metal formed with Al, Cr, and Cu metal powder addition.

Table 3. Weld metal compositions.

	%C	%Si	%Mn	* O	%Al	%P	%S	%Cr	%Cu	%Fe
Base Case	0.110	0.260	1.300	499	0.032	0.022	0.011	0.110	0.110	98.03
MP2	0.081	0.980	1.700	299	6.690	0.014	0.010	7.790	0.100	82.60
MP4	0.095	0.860	1.530	292	6.970	0.019	0.010	6.280	7.297	76.91

* ppm; % is in mass%.

Comparison of the BC and MP weld metal compositions in Table 3 shows that the levels of Si, Mn, Al, and Cr increased in the MP2 weld metal. These elements also increased in the MP4 weld metal, as did the level of Cu. Therefore, the alloying of MP2 and MP4 weld metal from the added metal powders was successfully applied in these SAW experiments. The total oxygen content in the MP welds is similar at 299 ppm O and 292 ppm O, compared to the BC weld metal at 499 ppm, indicating acceptable oxygen control with the addition of Al as de-oxidizer in SAW.

Increased Si, Mn, Al, Cr, and Cu contents in the MP4 weld metal in the bulk analysis in Table 3 is confirmed in the EDS analyses of the weld metal as displayed in Table 4, for the different areas as indicated in the SEM micrographs in Figure 1.

Table 4. SEM-EDS analyses of areas in Figure 1 (mass%).

	Si	Mn	Al	Cr	Fe	Cu
a	0.86	1.63	5.64	7.11	77.9	6.9
b	0.89	1.57	5.68	7.01	78.3	6.5
c	0.83	1.54	5.63	6.88	78.9	6.2

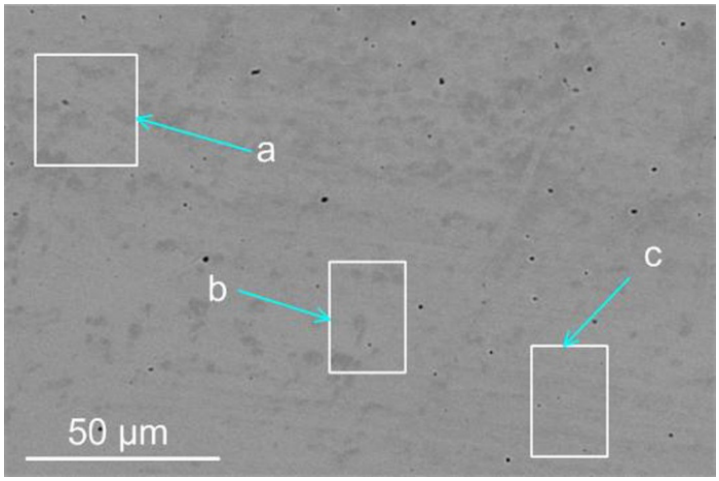

Figure 1. SEM BSE (backscattered electron) micrograph of weld metal analyzed areas (×1500).

Comparison of the post-weld slag bulk analysis in Table 5 for the base case to the MP2 and MP4 slags confirms that MnO and SiO_2 were reduced by Al metal powder at the weld pool-molten flux interface. The result is an increase in Al_2O_3 content in the MP2 and MP4 slags, also confirmed in Table 5 analyses.

Table 5. Post-weld slag compositions (mass%) *.

	MnO	CaO	SiO_2	Al_2O_3	CaF_2	MgO	FeO	Na_2O	Cu	CrO
Base Case	6.5	2.3	19.8	25.9	14.3	23.3	4.4	2.2	0.0	0.0
MP2	3.2	3.3	11.1	41.3	8.8	19.5	2.3	1.4	0.0	8.4
MP4	3.3	2.5	10.2	39.1	8.4	19.4	2.6	1.1	6.1	6.5

* mass% K_2O < 0.2 & mass% TiO_2 < 1.0%.

Even though Al is a strong de-oxidizer element, sufficient contact time between the Al powder and the molten flux is required to reduce MnO and SiO_2 via reactions (2) and (3). Similar Al_2O_3 forming reactions in the reduction of FeO, CrO and Cr_2O_3 should be considered as displayed in reactions (4)–(6). The reaction enthalpy values at 2000 °C for reactions (2) to (6) are shown next to each reaction. These reaction enthalpy values were calculated in FactSage 7.3 [32]. Besides the reduction reactions (2)–(6), the role of Al is to maintain a low oxygen potential at the molten flux-weld pool interface to prevent significant oxidation of Cr powder to Cr-oxides so that maximum Cr metal powder is transferred into the weld pool is ensured [33].

$$3(SiO_2) + 4(Al) = 3(Si) + 2(Al_2O_3) \qquad \Delta H_{2000\,^\circ C} = -82.1\ \text{kJ/mol Al} \tag{2}$$

$$3(MnO) + 2(Al) = 3(Mn) + (Al_2O_3) \qquad \Delta H_{2000\,^\circ C} = -248.4\ \text{kJ/mol Al} \tag{3}$$

$$3(FeO) + 2(Al) = 3(Fe) + (Al_2O_3) \qquad \Delta H_{2000\,^\circ C} = -416.5\ \text{kJ/mol Al} \tag{4}$$

$$3(CrO) + 2(Al) = 3(Cr) + (Al_2O_3) \qquad \Delta H_{2000\,^\circ C} = -326.6\ \text{kJ/mol Al} \tag{5}$$

$$(Cr_2O_3) + 2(Al) = 2(Cr) + (Al_2O_3) \qquad \Delta H_{2000\,^\circ C} = -256.3\ \text{kJ/mol Al} \tag{6}$$

( ): liquid.

It is well known from previous studies that large quantities of oxygen from flux oxide dissociation in the arc plasma is transferred via molten weld wire droplets to the arc plasma-weld pool interface, where this oxygen and iron react to form FeO in the colder weld pool steel. The established correlation is that the weld metal ppm O increased with increased FeO in the molten flux [11–16]. The slag analyses in Table 5 shows lowered FeO content in the MP slags, as compared to the BC slag. Therefore, it appears that the oxygen potential prevailing at the molten flux-weld pool interface is lowered by adding Al powder to reduce FeO via reaction (4). Since the bulk of the input chromium powder is added into the weld metal it can be deduced that the partial oxygen potential control via reaction (4) sufficiently shielded chromium metal powder from oxidation. If any CrO and/or Cr_2O_3 were formed, these oxides were easily reduced by Al according to reactions (5) and/or (6) to ensure that most of the input chromium powder was melted into the weld pool as elemental chromium.

Because the level of oxygen analyzed in MP2 and MP4 weld metal analyses are small, at only ppm quantities, as compared to the mass% Cr in the weld metal, very little of the Cr in the weld metal can be present as oxides in the weld metal.

4. Discussion

The total oxygen content in MP2 and MP4 weld metal are at similar levels (299 ppm O vs. 292 ppm O), confirming the function of the added Al metal powder in controlling the oxygen potential at the molten flux-weld pool interface. However, it appears that modification of the governing reactions occurred due to Cu powder addition in MP4 weld metal because the MP4 weld metal has increased Al content associated with a significant Cu uptake in the weld metal.

In the following section, the mass balance for each welding experiment is made to calculate the mass of each metal powder added into the weld metal. The total mass of metal added to each welded plate was recorded from pre- and post-weld plate mass measurements. The areas above and below the base plate level were measured to determine the dilution ratio. Figure 2 shows photograph images of the weld metal cross sections used in area proportion measurements. Areas were measured from stereoscope images, using the stereoscope suppliers' computer software.

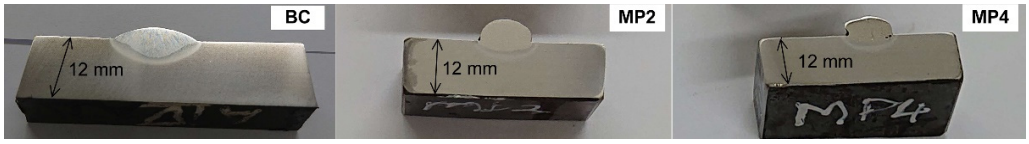

Figure 2. Photograph images of weld metal cross sections of BC, MP2, and MP4 weld metal.

The dilution ratio percentage, incorporating the metal powder contribution to the weld metal as ($\%DR_{(wire+MP)}$) is calculated as shown in Equation (7) [34]. This method is similar to the literature reported method applied in the case of weld wire and base plate used in bead-on-plate SAW [30,34]. In this method, the weld metal cross section area extending above the base plate level represents the proportion contribution of weld wire to the total weld metal mass. When metal powders and weld wire are added into the weld metal, the weld metal cross section area extending above the base plate level represents the proportion contribution of both, the metal powder, and the weld wire, to the total weld metal mass. The mass of Al, Cr, and Cu added to the weld metal was calculated from Equations (7)–(9), using the weld metal composition in Table 3 as input to Equation (9).

$$\%DR_{(wire+MP)} = [(A_{(wire+MP)})/(A_{(wire+MP)} + A_{BP})] \times 100 \quad (7)$$

$$M_{WM} = (M_{wire} + M_{MP}) \times [100/(\%DR_{(wire+MP)})] \quad (8)$$

$$(\text{gram Al to WM}) = (M_{WM}) \times (\%Al_{WM}/100) \quad (9)$$

WM = weld metal; MP = metal powder; BP = base plate; Wire = weld wire; M = mass (gram); A = area (mm^2).

Table 6 shows the mass of each metal powder, and their sum, melted into the weld metal. The mass of Cr melted into MP2 and MP4 weld metal is similar. The mass of Al melted into the MP4 weld metal is higher compared to that of MP2. The total mass of metal powders melted into the MP4 weld metal is significantly higher compared to MP2 at 19.2 vs. 11.1 g. Increased metal powder was incorporated into the weld metal in MP4, compared to MP2, at the same welding energy input of 2.0 kJ/mm. This difference is due to the metal stabilizer role of copper as discussed below. Figures 3–6 were sourced from the FactSage 7.3 thermochemical databases and are used here to illustrate the chemical effect of Cu powder addition to the SAW welding process [32]. The melting point (liquidus temperature) of pure Al, Cr, and Cu are 660, 1857, and 1083 °C.

Table 6. Post weld masses and metal powder mass added to weld metal.

	Al (g)	Cr (g)	Cu (g)	* Powder (g)	Wire (g)	Base Plate (g)	Weld Metal (g)	Slag (g)	$\%DR_{(wire+MP)}$
Base Case	0	0	0	0	33.7	67.6	135		50
MP2	5.1	6.0	0	11.1	48.4	16.5	77	31.1	78
MP4	6.5	5.9	6.8	19.2	55.8	18.7	94	30.8	80

* Total Al, Cr, and Cu powder added to weld metal.

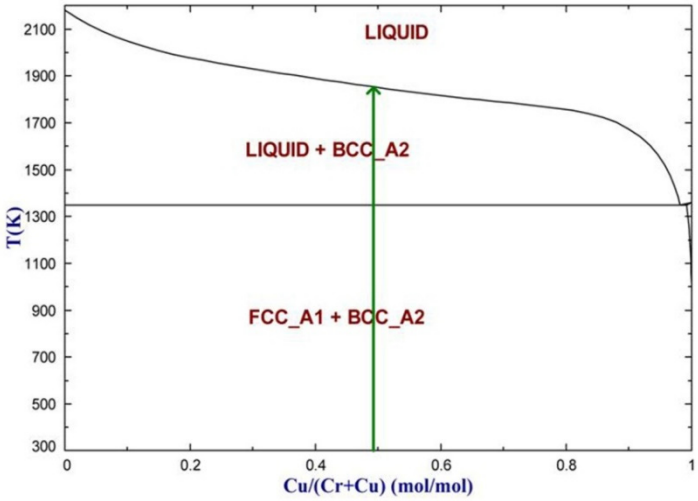

Figure 3. Cr-Cu phase diagram from FactSage 7.3 databases [32].

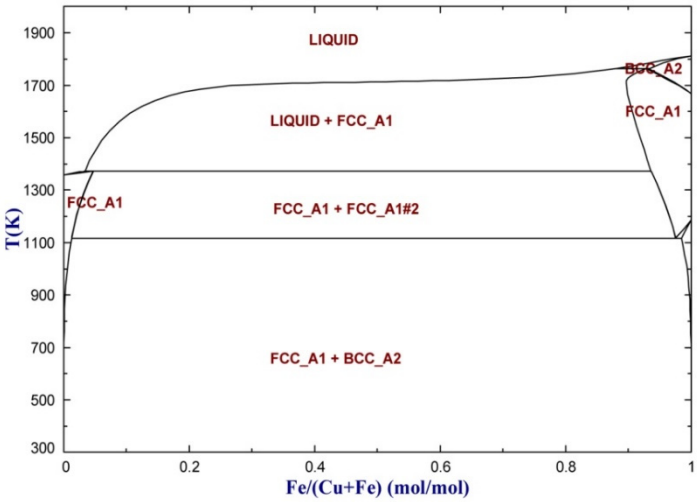

Figure 4. Cu-Fe phase diagram from FactSage 7.3 databases [32].

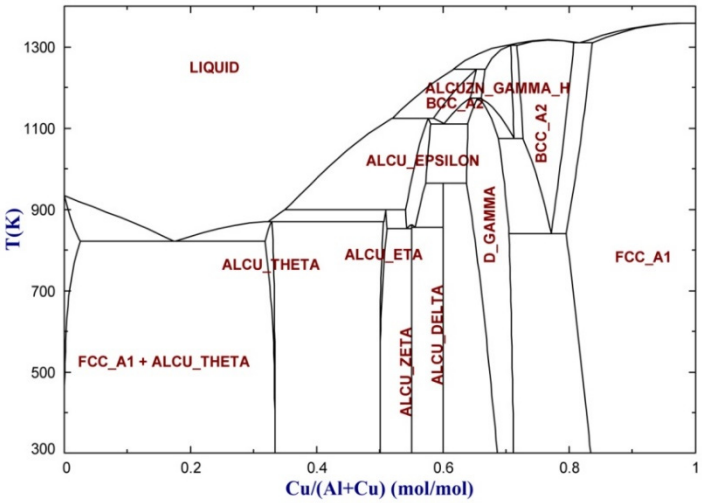

Figure 5. Cu-Al phase diagram from FactSage 7.3 databases [32].

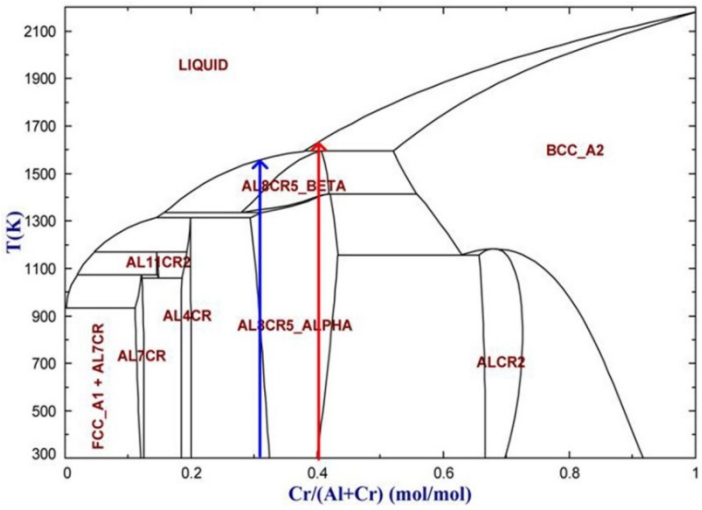

Figure 6. Cr-Al phase diagram from FactSage 7.3 databases [32].

The stabilizer effect by Cu is due to its lowering of the Cr liquidus temperature by 263 from 1857 to 1593 °C at the mol ratio of Cr/(Cu+Cr) = 0.49 at the green arrow in Figure 3, equivalent to 54 mass% Cu in Cu-Cr alloy. This mol ratio of Cr/(Cu+Cr) = 0.49 represents the MP4 alloy composition in Table 3. Therefore, due to the liquidus temperature lowering effect of Cu addition to pure Cr, the addition of Cu metal powder serves as stabilizer of Cr in the weld pool by decreasing the temperature required to melt Cr into the weld pool. Copper does not have the same drastic liquidus lowering effect on Fe or Al as is shown in the binary phase diagrams of Cu-Fe and Cu-Al in Figures 4 and 5. Since Cu does not have a high affinity for oxygen, as compared to Al, it stays in the weld pool as a metallic copper and remains viable throughout the welding process as a stabilizer element for Cr.

Although Al has a significant liquidus temperature lowering effect on Cr as shown in Figure 6, this effect is expected to be of the same magnitude in the MP2 and MP4 weld metals as marked at the stoichiometric mol ratio of Cr/(Al+Cr) at 0.41 (54 mass% Cr in Cr-Al alloy) for MP2 (red line) and at 0.32 (48 mass% Cr in Cr-Al alloy) for MP4 (blue line) at liquidus temperatures of 1327 vs. 1298 °C. Although similar quantities of Cr powder were melted into the MP2 and MP4 weld metal, more Al and the additional 6.8 g of Cu were melted into the MP4 weld pool. Therefore, the interaction between the powdered alloying additions to form an initial low melting alloy most likely served to enhance the overall increase in MP4 powder melt mass, compared to that in MP2.

The Cr-Al-Cu liquidus projection lines in Figure 7 confirm this effect. The composition point (filled round marker) in Figure 7 is the endpoint proportions of Cr-Al-Cu, at a liquidus temperature of 1250–1300 °C, similar to the liquidus temperature of 1298 °C marked in the Cr-Al phase diagram in Figure 6. According to the liquidus projection lines in Figure 7, the effect of increased Cu pick-up in the starting binary alloy of Cr-Al can be seen. Starting with the binary alloy of mol ratio Cr/(Al+Cr) at 0.32 for MP4, equivalent to 52% Al–48% Cr composition point as marked by the arrow point on the Cr-Al axis in Figure 7, increased copper content to the end-point composition will be 100% liquid at 1350 °C at low copper content values, and 100% liquid at 1250 °C at the end-point copper content for the ternary alloy of Cr-Al-Cu, indicated by the filled circle icon. Therefore, more weld wire may be melted into the initially formed Cr-Al-Cu alloy of low melting point in MP4, as compared to the smaller volume of initial Cr-Al alloy formed in MP2.

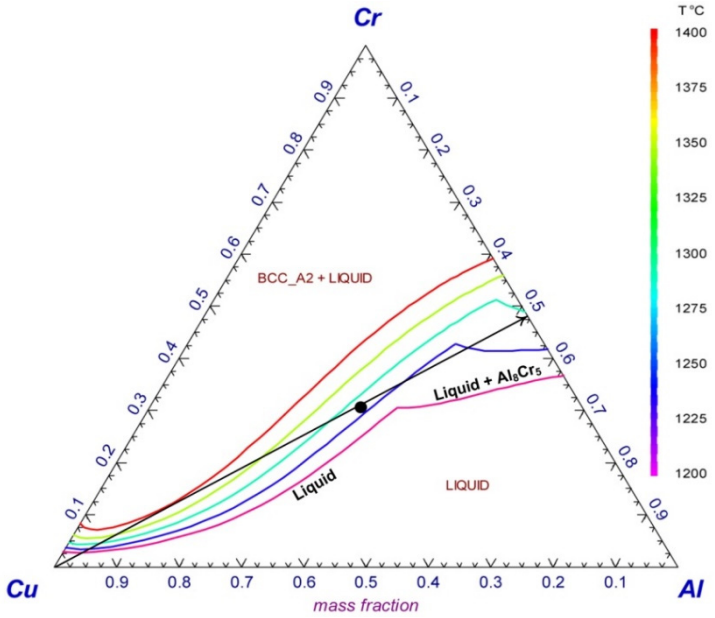

Figure 7. Cr-Al-Cu liquidus projection calculated in FactSage 7.3 [32].

In addition to the effect of Cu and/or Al in lowering the alloy liquidus temperature from that of pure Cr, the effect of the alloying elements on the weld pool metal solidus temperature is also important. The weld pool molten time can be extended if the weld pool steel chemistry is changed to a composition with a decreased solidus temperature. This solidus lowering effect by Cu, Al, and Cr alloying of the weld pool is confirmed in Figure 8. The solidification curve for MP4 weld metal shows the solidus temperature much below 1300 °C (solidus temperature of 1000 °C), compared to the solidus temperature of MP2 weld metal at 1407 °C. The Equilib module in FactSage 7.3 was applied to calculate the curves in Figure 8. The databases for oxides (FToxid) and steel (FSstel) were selected for these calculations.

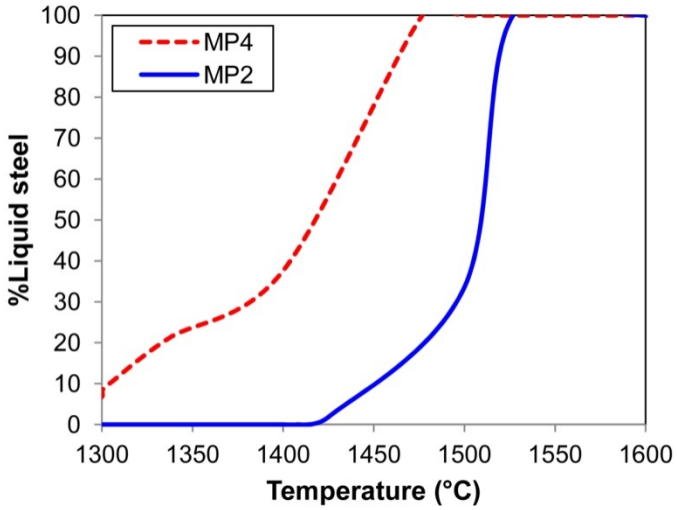

Figure 8. Solidification curves for MP2 and MP4 weld metal compositions calculated in FactSage 7.3 [32].

The MP weld metal analysis in Table 3 displays higher Mn and Si contents, as compared to the BC weld metal, and thus confirms that MnO and SiO_2 were reduced from the molten flux by added Al powder via reactions (2) and (3). Comparison of the post-weld slag analyses in Table 5 for BC to MP samples also confirm that SiO_2 and MnO were reduced by Al to form Al_2O_3 in the slag. Although the complex phase diagram for the flux system

used here is not available, several studies on the phase chemistry and physico-chemical properties of Al_2O_3-MgO-CaF_2-SiO_2-Na_2O-K_2O-Fe_2O_3 based fluxes were reported [35,36]. Because Al_2O_3 and MgO combine to form refractory Spinel phase ($MgO{\cdot}Al_2O_3$), and Alumina itself is also of high melting point, the addition of Al_2O_3 from the Al reduction reactions results in decreased slag fluidity. The practical effect of higher solids content of the slag is that the slag is not as easily detached from the weld metal as compared to the BC slag. Therefore, more CaF_2 addition to the flux is needed to increase the liquid phase proportion in the slag to maintain the same quantity solids phase of Spinel and Al_2O_3 in the MP slags as in the BC slag.

The following calculations were made to quantify the grams of MnO and SiO_2 reduced by Al according to reactions (2) and (3). Equation (10) was used to calculate the mass of Mn and Si added to the MP weld metals, compared to the BC weld metal nominal composition. The weld metal mass and the dilution ratio values in Table 6 were used as inputs to Equation (10). Equation (10) is expressed in terms of Mn to calculate the mass of Mn added to MP2 and MP4 weld metals, respectively. The square bracketed part of Equation (10) represents the BC weld metal nominal composition. The same expression as in Equation (10) can be applied to calculate the mass of Si added to MP2 and MP4 weld metals, respectively.

$$M_{Mn} = (M_{WM}) \times ((\%Mn_{WM}/100) - (\%DR_{wire}/100) \times (\%Mn_{wire}/100) - [1 - (\%DR_{wire}/100) \times (\%Mn_{BP}/100)]) \quad (10)$$

M = mass (gram); M_{MN} = mass Mn (gram); $\%Mn_{WM}$ = %Mn in weld metal; $\%DR_{wire}$ = % of weld metal contributed by weld wire in the Base Case (BC); $\%Mn_{wire}$ = %Mn in weld wire; $\%Mn_{BP}$ = %Mn in base plate (BP); WM = weld metal; BP = base plate; Wire = weld wire.

Table 7 shows the calculation results from Equation (10), expressed as the grams of SiO_2 and MnO reacted via reactions (2) and (3). The exothermic heat generated from reactions (2) and (3) are also displayed in Table 7. These values were calculated from the exothermic reaction heats values ($\Delta H_{2000^\circ C}$) for each reaction as displayed next to reactions (2) and (3) in Section 3. Table 7 also shows the increase in weld metal temperature expected from the kJ exothermic heat generated from reactions (2) and (3). The heat capacity of steel (0.460 kJ/kg K) was used to calculate the maximum weld metal temperature increase expected for the total kJ exothermic heat in Table 7. Since the exothermic heat generated from reactions (2) and (3) in both MP2 and MP4 weld metal is of the same magnitude (−3.4 and −3.6 kJ), the temperature increases in MP2 and MP4 weld metal are similar at 97 °C and 84 °C, respectively. Although reaction (4) must have occurred in order to control the partial oxygen pressure at the weld pool-slag interface, the extent of this reaction is not precisely known [37]. However, because the same welding parameter inputs and welding flux were used in the welding tests, the same quantity of oxygen must have been initially transferred to the weld pool from the weld wire metal droplets melted in the arc cavity. Because the same order of magnitude exothermic heat quantity was generated in MP2 and MP4 weld metal from reactions (2) and (3), and the same extent of rection (3) is expected since the same initial quantity of oxygen prevailed in the weld pool, reactions (2) to (4) are not likely the cause of the higher melting rate of metal powders into MP4 weld metal, compared to the metal powder melting rate into MP2 weld metal.

Table 7. Exothermic heat from reactions (2) and (3).

	SiO_2 (g)	MnO (g)	Al (g)	Reaction (2) (kJ)	Reaction (3) (kJ)	Reactions (2) & (3) (kJ)	Weld Metal ΔT (°C)
MP2	1.3	0.5	0.9	−2.3	−1.1	−3.4	97
MP4	1.4	0.4	1.0	−2.6	−1.0	−3.6	84

Figure 9 illustrates the reaction sites and reaction sequence in the SAW process for welding with Al, Cr, and Cu powder additions. The initial reaction steps of A to E1 are well

accepted in the published literature [2,7–9,13,34]. Previous studies demonstrated that the droplets of molten weld wire transfer large quantities of oxygen (2000–3000 ppm O) into the weld pool via the weld pool–arc plasma interface [7,8]. The molten weld wire droplets retained oxygen from the decomposition of less stable oxides in the arc plasma. Less stable oxides decompose more readily in the arc plasma due to the high temperatures prevailing in the arc plasma. Therefore, flux chemistry specification is an important control input in the SAW process to set the quantity of transferrable oxygen in the arc plasma [9]. The release of oxygen from the dissociation of the flux oxides is represented in reactions A to D.

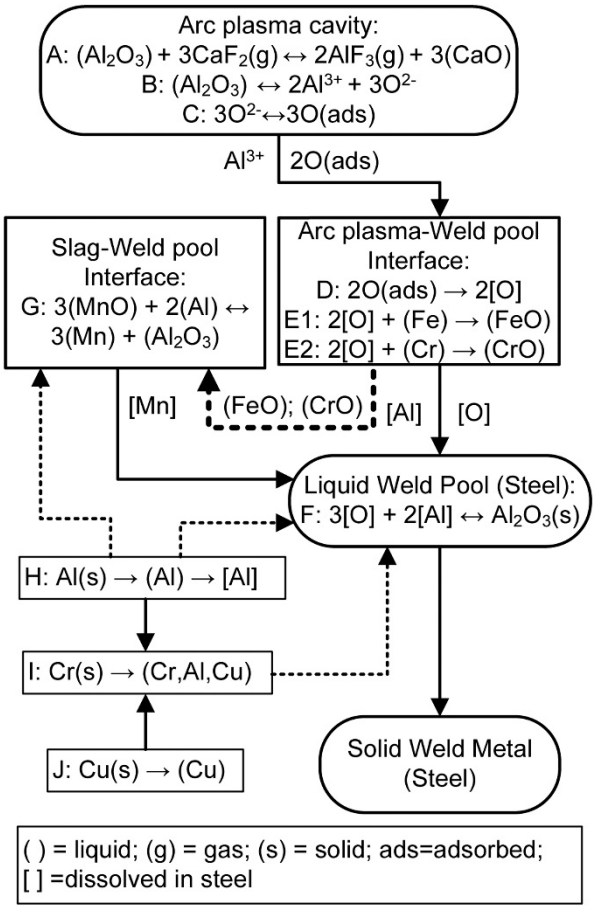

Figure 9. SAW reaction flow diagram with Al, Cr, and Cu powder addition reactions.

The excess oxygen is transferred via molten weld wire droplets from the arc cavity to the weld pool at the arc plasma–weld pool interface form FeO which floats to the weld pool–molten flux interface and is transferred into the molten flux. Increased FeO in the molten flux is associated with increased weld metal ppm O as reported in multiple studies in which post-weld slags (molten flux) were analyzed [11–16]. Chromium has a higher affinity for oxygen, compared to Fe, and it is expected that CrO will form at the arc plasma–weld pool interface where excess oxygen is added into the weld pool, and can react with dissolved elements in the weld pool. This reaction of CrO formation, reaction (E2), is similar to the FeO formation reaction (E1). The tendency of Cr to form Cr-oxides in SAW has been studied previously for the application of high Cr weld wires (1.4% Cr-26% Cr) in combination with Cr_2O_3 containing fluxes [12]. In this study, the FeO content on the post-weld slags ranged from 0.63% FeO to 5.18% FeO, indicating the oxidizing nature of the slag. The maximum %Cr added to the weld metal was 3.7%. This value is low given the high Cr_2O_3 content in the fluxes was at 10–18% Cr_2O_3, representing unit activity of Cr_2O_3 in the molten flux. Very high ppm O were analyzed in the weld metals at 470 ppm O to 1190 ppm O, indicating high levels of oxygen release from oxide decomposition in the

arc cavity. Therefore, the oxygen potential must be lowered by lowering the excessive ppm O from the arc cavity to ensure that Cr is transferred into the weld metal. Despite addition of Al powder to complete this function, some FeO and CrO remains in the post weld slag (Table 5).

The oxygen potential prevailing at the molten flux-weld pool interface, as presented by the quantity of FeO and/or CrO, is reduced in this work by adding Al powder. Similar to reaction G for reduction of MnO from the molten flux, FeO is also reduced by Al, see reaction (4). If CrO or Cr_2O_3 formed at the arc plasma-weld pool interface, these oxides would be reduced to Cr metal according to reactions (5) and (6). The oxidation of Cr to Cr-oxides at the molten flux–weld pool interface is limited due to the deoxidizer effect of Al in reducing the oxygen potential at this reaction interface. Consequently, the added Cr metal powder remains in the metallic chromium form, and is available to alloy with Al and Cu, reaction I in Figure 9.

Furthermore, the exothermic reactions of MnO, SiO_2, FeO, and Cr-oxides with Al, reactions (2) to (6), add heat to the weld pool to further facilitate melting and dissolution of Cr. Because an excess of Al powder is added to the SAW process, a large quantity of Al dissolves into the weld pool, reaction H in Figure 9. Some of this Al reacts with oxygen in the steel to form Al_2O_3 inclusions, reaction F.

The relatively high weld metal total oxygen content level of 299 ppm O indicates that weld metal oxygen content is not only set by equilibrium deoxidation reactions when Al and Cr metal powders are added to the molten flux-weld pool interface because much lower ppm O is expected in equilibrium with steel containing percentage quantities of Al and Cr, as is the case for MP2 and MP4 weld metal (Table 3). For comparison, the equilibrium dissolved ppm O from literature for similar chromium containing alloys are less than 30 ppm O for 1% Al in the alloy at 1600 °C [38]. Thermochemical modeling of the SAW process confirmed that gas-slag-metal equilibrium prevails in the SAW process in the absence of metal powder additions [11,39]. Since relatively high ppm O is attained in the MP weld metals in the presence of high Al and Cr content in the weld metal, it appears that the same mechanism of oxygen transfer from the arc cavity to the weld pool occurs when Al, Cr, and Cu metal powders are added to the SAW process. Recent work confirmed this mechanism of oxygen transfer from the arc cavity to the weld pool via molten weld wire droplets [2]. Furthermore, spectroscopy measurements showed that Na, Ca, Mn, and Fe metal vapors were present in the arc cavity [2]. Despite the presence of high oxygen affinity metal vapors of Ca, Mn, and Fe, these elements were inadequate in contact and/or quantity to prevent pick-up of oxygen in the molten weld wire droplets, and oxygen transfer via the droplets into the weld pool. Therefore, in agreement with this work and other studies, it is clear that the transfer of high oxygen affinity elements into the weld pool requires oxygen potential control at the weld pool-molten slag interface and cannot be controlled in the arc cavity only. The droplet ppm O content is influenced by flux chemistry, but it may be drastically altered by different welding parameters, resulting in higher or lower arc cavity temperatures, and thus higher or lower extents of oxide dissociation. Higher ppm O were measured in the droplets and weld metal in the case of use of DCEP (direct current electrode positive) at 600 and 1000 A linked to higher arc cavity temperatures vs. lower ppm O for DCEN (direct current electrode negative) and alternating current linked to lower cavity temperatures [2].

The results presented here confirm the feasibility of using unconstrained Al powder additions in SAW to reduce the oxygen potential at the molten flux-weld pool interface to achieve increased metal transfer from metal powders to the weld pool. This method of oxygen control does not interfere with the accepted oxygen transfer mechanism in SAW, namely oxygen transfer from the arc plasma to the weld pool, via molten metal droplets through the weld pool–arc plasma interface. The importance of this oxygen potential control method is to ensure sufficiently reducing conditions at the molten flux-weld pool interface to maintain unconstrained Cr powder in the metallic form to enable Cr-Al-Cu alloy stabilization for increased metal transfer into the weld pool.

5. Conclusions

1. Application of unconstrained (not fluxed cored or metal cored wire) metal powders of Al in combination with Cr and Cu is demonstrated for the submerged arc welding process;
2. Al powder is applied as de-oxidizer element to control the oxygen potential at the molten flux–weld pool interface to ensure transfer chromium (a high oxygen affinity element) into the weld pool;
3. Application of Al-Cr powders achieved alloying of 6.69% Al and 7.79% Cr and application of Al-Cr-Cu powders achieved 6.97% Al, 6.28% Cr and 7.30% Cu for the same welding parameters of 500 A (direct current electrode positive), 28 V, and 42 cm/minute travel speed;
4. Weld metal total oxygen was controlled to 292 and 299 ppm O when Al powder additions were applied, vs. 499 ppm O in the absence of metal powder;
5. More metal powder mass was melted into the weld pool with Cr-Al-Cu powders added, compared with Cr-Al powder addition;
6. This study illustrates the application of copper as stabilizer, in conjunction with aluminum, to enhance chromium transfer to the weld pool. The stabilizer effect occurs because the Cr-Al-Cu alloy liquidus temperatures are much lower than the pure Cr liquidus temperature. Weld pool cooling time, as set by the temperature interval between the alloyed weld metal pool liquidus and solidus temperatures, is significantly increased with Cr-Al-Cu metal powder addition, as compared to Cr-Al metal powder addition;
7. The bulk of Al_2O_3 formed in the exothermic reduction of oxides at the weld pool-molten flux interface was absorbed into the molten flux and altered the molten flux (slag) properties. For example, slag fluidity was decreased due to increased sold phase content (Spinel), and consequently the post-weld slag detachment extent decreased.

Author Contributions: F.D.B. conceptualized the work; F.D.B. and T.C. executed the experiments, interpreted the data, and prepared the manuscript. All authors have read and agreed to the published version of the manuscript.

Funding: This research was funded in part by the National Research Foundation of South Africa, grant number BRIC171211293679.

Institutional Review Board Statement: Not applicable.

Informed Consent Statement: Not applicable.

Data Availability Statement: The data presented in this study are available on request from the corresponding author.

Conflicts of Interest: The authors declare no conflict of interest. The funders had no role in the design of the study; in the collection, analyses, or interpretation of data; in the writing of the manuscript, or in the decision to publish the results.

References

1. Sengupta, V.; Havrylov, D.; Mendex, P.F. Physical phenomena in the weld zone of submerged arc welding—A Review. *Weld. J.* **2019**, *98*, 283–313.
2. Gött, G.; Gericke, A.; Henkel, K.-M.; Uhrlandt, D. Optical and spectroscopic study of a submerged arc welding cavern. *Weld. J.* **2016**, *95*, 491–499.
3. Chai, C.S.; Eagar, T.W. Slag-metal equilibrium during submerged arc welding. *Metall. Trans. B* **1981**, *12*, 539–547. [CrossRef]
4. Mitra, U.; Eagar, T.W. Slag-metal reactions during welding: Part I. Evaluation and reassessment of existing theories. *Metall. Trans. B* **1991**, *22*, 65–71. [CrossRef]
5. Eagar, T.W. Sources of weld metal oxygen contamination during submerged arc welding. *Weld. J.* **1978**, *57*, 76–80.
6. Tuliani, S.S.; Boniszewski, T.; Eaton, N.F. Notch toughness of commercial submerged arc weld metal. *Weld. Met. Fabr.* **1969**, *37*, 327–339.
7. Polar, A.; Indacochea, J.E.; Blander, M. Electrochemically generated oxygen contamination in submerged arc welding. *Weld. J.* **1990**, *69*, 68–74.

8. Lau, T.; Weatherly, G.C.; Mc Lean, A. The sources of oxygen and nitrogen contamination in submerged arc welding using CaO-Al_2O_3 based fluxes. *Weld. J.* **1985**, *64*, 343–347.
9. Chai, C.S.; Eagar, T.W. Slag metal reactions in binary CaF_2-metal oxide welding fluxes. *Weld. J.* **1982**, *61*, 229–232.
10. Dallam, C.B.; Liu, S.; Olson, D.L. Flux composition dependence of microstructure and toughness of submerged arc HSLA weldments. *Weld. J.* **1985**, *64*, 140–152.
11. Coetsee, T.; Mostert, R.J.; Pistorius, P.G.H.; Pistorius, P.C. The effect of flux chemistry on element transfer in Submerged Arc Welding: Application of thermochemical modelling. *J. Mater. Res. Technol.* **2021**, *11*, 2021–2036. [CrossRef]
12. Mitra, U.; Eagar, T.W. Slag metal reactions during submerged arc welding of alloy steels. *Metall. Trans. B* **1984**, *15*, 217–227. [CrossRef]
13. Mitra, U.; Eagar, T.W. Slag-metal reactions during welding: Part II. Theory. *Metall. Trans. B* **1991**, *22*, 73–81. [CrossRef]
14. Zhang, J.; Coetsee, T.; Wang, C. Element transfer behaviors of fused CaF_2-SiO_2 fluxes subject to high heat input submerged arc welding. *Metall. Trans. B* **2020**, *51*, 16–21. [CrossRef]
15. Zhang, J.; Coetsee, T.; Dong, H.; Wang, C. Element transfer behaviors of fused CaF_2-SiO_2-MnO fluxes under high heat input submerged arc welding. *Metall. Trans. B* **2020**, *51*, 885–890. [CrossRef]
16. Zhang, J.; Coetsee, T.; Dong, H.; Wang, C. Element Transfer Behaviors of fused CaF_2-TiO_2 Fluxes in EH36 Shipbuilding steel during high heat input Submerged Arc Welding. *Metall. Trans. B* **2020**, *51*, 1953–1957. [CrossRef]
17. ESAB. Available online: http://assets.esab.com/asset-blank/assetfile/12295.pdf (accessed on 13 June 2021).
18. Chovet, A.; Galand, E.; Leduey, B. Effect of various factors on toughness in P92 SAW weld metal. *Weld. World* **2008**, *52*, 18–26. [CrossRef]
19. O'Brien, A. Welding Processes, Part 1. In *Welding Handbook*, 9th ed.; American Welding Society (AWS): Miami, FL, USA, 2004; Volume 2, pp. 256–297.
20. De, S.K.; Srikanth, S.; Saxena, A.K.; Jha, B.K. Copper bearing steels from SAIL and its application. *Int. J. Metall. Eng.* **2016**, *5*, 1–8.
21. Patel, D.; Soman, S.N. Develop a flux cored wire for submerged arc welding of Ni-Mo low alloy steel. *Sadhana* **2020**, *45*, 127. [CrossRef]
22. Raabe, D.; Tasan, C.C.; Springer, H.; Bausch, M. From high-entropy alloys to high-entropy steels. *Steel Res. Int.* **2015**, *86*, 1127–1138. [CrossRef]
23. Jain, H.; Shadangi, Y.; Shivam, V.; Chakravarty, D.; Mukhopadhyay, N.K.; Kumar, D. Phase evolution and mechanical properties of non-equiatomic Fe-Mn-Ni-Cr-Al-Si-C high entropy steel. *J. Alloys Compd.* **2020**, *834*, 155013. [CrossRef]
24. Moon, J.; Ha, H.-Y.; Kim, K.-W.; Park, S.-J.; Lee, T.-H.; Kim, S.-D.; Jang, J.H.; Jo, H.-H.; Hong, H.-U.; Lee, B.H.; et al. A new class of lightweight, stainless steels with ultra-high strength and large ductility. *Sci. Rep.* **2020**, *10*, 12140. [CrossRef]
25. Gehling, T.; Treutler, K.; Wesling, V. Targeted influence on the weld strength of high-strength fine-grain structural steels in the GMA welding process through functionalized weld metal surfaces. *Weld. World* **2019**, *63*, 783–792. [CrossRef]
26. Bailey, N. Submerged Arc Welding ferritic steels with alloyed metal powder. *Weld. J.* **1991**, *70*, 187–206.
27. Nand, S.; Singh, P.K. Effect of addition of metal powder on deposition rate, mechanical properties, and metallographic property of weld joints during Submerged Arc Welding process. *J. Mach. Form. Technol.* **2015**, *6*, 159–168.
28. Tušek, J.; Suban, M. High-productivity multiple-wire Submerged-Arc Welding and cladding with metal-powder addition. *J. Mater. Process. Technol.* **2003**, *133*, 207–213. [CrossRef]
29. Bong, W.L. System and Method for Metal Powder Welding. U.S. Patent 8946582 B1, 3 February 2015.
30. Coetsee, T.; De Bruin, F. Application of Copper as Stabiliser in Aluminium Assisted Transfer of Titanium in Submerged Arc Welding of Carbon Steel. *Processes* **2021**, *9*, 1763. [CrossRef]
31. Coetsee, T. Phase chemistry of Submerged Arc Welding (SAW) fluoride based slags. *Mater. Res. Technol.* **2020**, *9*, 9766–9776. [CrossRef]
32. Bale, B.R.; Chartrand, P.; Degterov, S.A.; Errikson, G. FactSage thermochemical software and databases. *Calphad* **2002**, *26*, 189–228. [CrossRef]
33. Coetsee, T.; De Bruin, F.J. Reactions at the molten flux-weld pool interface in submerged arc welding. *High Temp. Mater. Process.* **2021**, *40*, 421–427. [CrossRef]
34. Indacochea, J.; Blander, M.; Christensen, N.; Olson, D. Chemical reactions during Submerged Arc Welding with FeO-MnO-SiO_2 fluxes. *Metall. Trans. B* **1985**, *16*, 237–245. [CrossRef]
35. Sokolsky, V.E.; Roik, O.S.; Davidenko, A.O.; Kazimirov, V.P.; Lisnyak, V.V.; Galinich, V.I.; Goncharov, I.A. The phase evolution at high-temperature treatment of the oxide-fluoride ceramic flux. *Res. J. Chem. Sci.* **2014**, *4*, 71–77.
36. Davidenko, A.O.; Sokolsky, V.E.; Lisnyak, V.V.; Roik, O.S.; Goncharov, I.A.; Galinich, V.I. The effect of spinel formation in the ceramic welding fluxes on the properties of molten slag. *Res. J. Chem. Sci.* **2015**, *5*, 23–31.
37. Coetsee, T.; De Bruin, F.J. Improved titanium transfer in Submerged Arc Welding of carbon steel through aluminium addition. In *Mineral Processing and Extractive Metallurgy Review*; Taylor & Francis Online: Abingdon, UK, 2021.
38. Lee, S.; Choi, J.; Jung, S.; Lee, H.; Rhee, P. Aluminium deoxidation equilibrium of liquid Fe-16 Pct Cr alloy. *Metall. Trans. B* **2005**, *36*, 414–416. [CrossRef]
39. Zhang, J.; Coetsee, T.; Basu, S.; Wang, C. Impact of gas formation on the transfer of Ti and O from TiO_2-bearing basic fluoride fluxes to submerged arc welded metals: A thermodynamic approach. *Calphad* **2020**, *71*, 102195. [CrossRef]